NJC

Accepted Manuscript

This article can be cited before page numbers have been issued, to do this please use: X. Ma, J. Cheng, J. Liu, X. Zhou and H. Xiang, *New J. Chem.*, 2014, DOI: 10.1039/C4NJ01908C.

View Article Online
DOI: 10.1039/C4NJ01908C

Journal Name

RSC Publishing

ARTICLE

Ratiometric fluorescent pH probes based on aggregation-induced emission-active salicylaldehyde azines

Cite this: DOI: 10.1039/x0xx00000x

Xiaofeng Ma, Jinghui Cheng, Jiaoyan Liu, Xiangge Zhou and Haifeng Xiang*

Received 00th January 2012,
Accepted 00th January 2012

DOI: 10.1039/x0xx00000x

www.rsc.org/

A series of luminescent salicylaldehyde azines (SAs) containing different electron-accepting substituents (–NO_2, –F, and –Cl), electron-donating substituents (–OMe and –NEt_2), and π-extended system (naphthalene ring) are prepared for the application of fluorescent pH probes. These SAs inheriting the aggregation-induced emission (AIE) features display strong blue, green, and red fluorescence with large Stokes shifts in water and solid. Combining advantages of AIE and chemical reactivity of phenol towards OH^-/H^+, most of the SAs can be used as ratiometric fluorescent pH probes with a broad pH range (2–14) in water and solid (test paper). Moreover, the inherent relationships between their chemical structures and AIE properties/pK_a values (7.5–13.3) are studied, which provide unequivocal insights for the design of AIE-active dyes and their applications.

Introduction

Protons are one of the most important targets of interest, because many biological and geochemical processes occurring in freshwater, seawater, and marine sediments involve strong pH changes. Accordingly, the recognition and detection of pH values have been an especially active research area. The most traditional pH measurement is glass electrode, however, it has some obvious disadvantages including single point measurements and bulky and invasive properties for the bio-applications.[1] Recently, fluorescent pH probes have attracted considerable interests, because fluorescence detections allow noninvasive measurements with biological objects, parallel monitoring of multiple samples, and imaging.[2] The most common fluorescence detection is the measurement of fluorescence intensity, but, in most cases, its determination accuracy is frequently compromised by ambient or scattered light, instrumental fluctuation, and background fluorescence. Therefore, ratiometric fluorescent measurement is more desired.[3] Moreover, it usually provides the perceived colour change, which would be useful for the rapid visual sensing. In general, most of the reported ratiometric fluorescent pH probes employ mixture of different fluorescent dyes[4] or a single fluorescent dye containing different multiple pH-sensitive segments.[1,5] Both of them might have some shortcomings, such as unequal stability, reliability, and photobleaching of the different dyes or segments. Another simpler and more efficient method is to design and synthesize a single fluorescent dye that has only one kind of pH-sensitive segment that can emit light at different wavelengths after deprotonation or protonation. Up to now, this kind of probes are much scarcer,[6] because a fluorescent dye containing only one kind of pH-sensitive segment usually would tend to quench or enhance fluorescence, whithout ratiometric fluorescence after deprotonation or protonation.

For pH detection applications, the preferred work conditions are aqueous media, but it is incongruous that most organic fluorescent dyes are hydrophobic aromatics that are barely soluble in water. Introduction of hydrophilic groups would improve their aqueous solubility improved, meanwhile, the resulting amphiphilic dyes would be ready to aggregate in water and lead to fluorescence quenching by the aggregation-caused quenching (ACQ) effect. Tang et. al. recently discovered an exactly opposite phenomenon of aggregation-induced emission (AIE).[7] Since then a large number of AIE-active dyes have been developed and used in organic light-emitting diodes, bio/chemosensors, bioimaging, and so on.[8]

Our previous work focused on the synthesis, photophysical properties, and sensing applications of salicylaldehyde-based Salen Schiff bases (Scheme 1).[9] Most of these Salen Schiff bases usually exhibit much stronger fluorescence in organic solution than in solid or water, indicating the possible existence of ACQ. On the other hand, salicylaldehyde azines (SAs) (Scheme 1) explored by Tong et. al. have similar synthetic process and chemical structures with Salen Schiff bases but exhibit AIE effects.[10] Unlike the most common AIE-active dyes of tetraphenylethene (TPE), SAs have some unique properties: (1) two salicylaldimine moieties are connected by rotatable N–N single bond rather than C–C bond; (2) the rotations are

View Article Online
DOI: 10.1039/C4NJ01908C
Journal Name

restricted in the N–N bond only by intramolecular hydrogen bonds;[10a] (3) the intramolecular hydrogen bonds lead to keto and enol tautomers for SAs through an ultrafast excited-state intramolecular-proton transfer (ESIPT) process.[11] Furthermore, SAs have been used as fluorescent probes for the detection of Zn^{2+},[12] Co^{2+},[12b] Cu^{2+}, Fe^{3+},[13] F^-,[14] CN^-,[15] protein,[16] and heparin.[17] At present, there are only limited examples of the AIE-active dyes for fluorescent pH sensing applications in the literature.[5a,18] In this work, we have systematically investigated the fluorescent pH sensing properties of a series of AIE-active SAs containing different electron-accepting (EA) substituents (–NO_2, –F, and –Cl), electron-donating (ED) substituents (–OMe and –NEt_2), and π-extended system (naphthalene ring) (Scheme 1), which provide a new paradigm in the design of ratiometric fluorescent pH probes. The photophysical properties of most SAs have not been examined and **3-F** has not been reported.

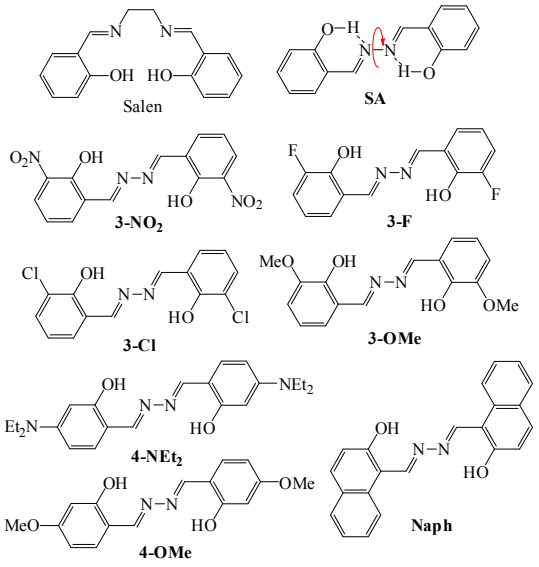

Scheme 1 Chemical structures of Salen and SAs.

Results and discussion

Synthesis and characterization

The general method of preparation of SAs is quite straightforward and consists of the condensation reaction of primary hydrazine with 2 equiv of salicylaldehyde precursor in ethanol under refluxing conditions, according to the previous report.[19] Most SAs have good solubility in organic solvents including DMSO and MeCN but poor solubility in water.

Photophysical and AIE properties

Among these SAs, the photophysical properties of **SA**,[10a] **4-NEt_2**,[20] and **Naph**[12b] have been examined and reported. As shown in Fig. 1 and Table 1, except **3-OMe** and **4-NEt_2**, all other SAs exhibit obvious AIE effects that the fluorescence in organic solvent is much weaker than that in solid or water. As example, the absorption and emission spectra of **SA** are depicted in Fig. 2. At room temperature, the dilute solution **SA** in MeCN emits very weak fluorescence (Fig. 2a) with a large Stokes shift and low quantum yield (Φ of 0.002, which might be contributed to the rotation of N–N single bond and the ESIPT process).[11] This ESIPT process is further confirmed by the pronounced solvatochromic effect (Fig. S1 in Supporting Information). However, if water was added to MeCN, the aggregate form of **SA** will be generated to eliminate the above effects, which results in AIE with a much higher Φ of 0.11 at a volume fraction (*f*) of water of 92 % (Fig. 2b). Moreover, absorption spectrum of **SA** in MeCN/water (*f* = 92 %) shows an obvious tail in the visible region, indicating the formation of aggregate nanoparticles.[10a]

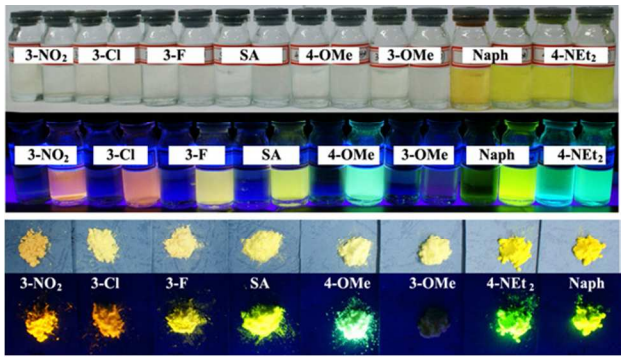

Fig. 1 Photographs (top: under sunlight; bottom: under 360 nm UV light) of the SAs in solution (left: MeCN; right: MeCN/water) and solid.

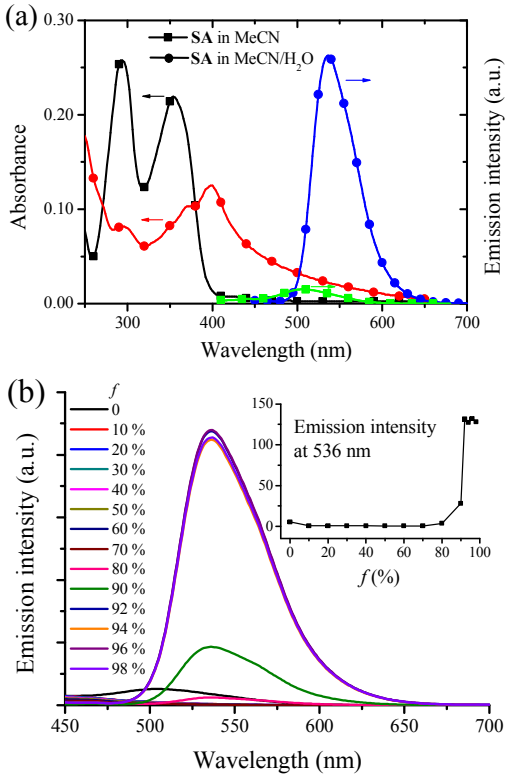

Fig. 2 (a) Absorption and emission spectra of **SA** in MeCN (1.0×10^{-5} mol dm^{-3}) and MeCN/H_2O (1.0×10^{-5} mol dm^{-3}, *f* = 92 %). (b) Emission spectra of **SA**

Journal Name

View Article Online
DOI: 10.1039/C4NJ01908C

MeCN/H_2O with different f (1.0×10^{-5} mol dm^{-3}); insert: plot of emission intensity at 536 nm with different f.

Table 1 Photophysical data of the organic molecules at room temperature.

	Medium	λ_{abs} /nm (ε /dm^3 mol^{-1} cm^{-1})	λ_{em} /nm	Φ	pK_a	f/%
SA	MeCN	292 (2.53×10^4); 354 (2.15×10^4)	509	0.002		
	water	296; 400	536	0.11	9.3	92
	solid		537			
3-NO_2	MeCN	270 (2.19×10^4); 364 (1.29×10^4); 504 (9.50×10^3)	543	0.004		
	water	395	565	0.04	7.5	90
	solid		566			
3-F	MeCN	300 (3.76×10^4); 350 (2.11×10^4)	518	0.002		
	water	402	547	0.05	8.2	92
	solid		550			
3-Cl	MeCN	302 (3.01×10^4); 354 (1.97×10^4)	513	0.003		
	water	302; 398	564	0.13	8.5	94
	solid		565			
3-OMe	MeCN	302 (3.01×10^4); 354 (1.97×10^4)	406	0.004		
	water	316; 408	-[a]	-[a]	-[a]	-
	solid		-[a]			
4-OMe	MeCN	308 (1.55×10^4); 362 (4.71×10^4)	488	0.003		
	water	300; 340	507	0.16	9.5	92
	solid		508			
4-NEt_2	MeCN	416 (8.07×10^4); 432 (7.59×10^4)	480	0.13		
	water	408; 426; 456	513	0.10	13.0	90
	solid		529	0.30[b]		
Naph	MeCN	330 (1.51×10^4); 406 (3.26×10^4); 424 (2.74×10^4)	510	0.004		
	water	334; 428; 462	530	0.18	13.3	80
	solid		536			

[a] nonemissive; [b] from Ref. 20a

The absorption and emission spectra of other SAs in MeCN are shown in Fig. S2 and S3. Since, except **4-NEt_2**, all other SAs in MeCN have very weak fluorescence (Table 1), the discussion will be focused on their AIE characteristics. As shown in Fig. 3, for aggregate SAs in MeCN/water and solid, different substituents have different effects on the emission peek (λ_{em}). Compared with the simplest **SA**, **4-OMe**, **4-NEt_2**, and **Naph** containing ED substituents or π-extended system show blue-shifted emission, on the contrary, **3-F**, **3-Cl**, and **3-NO_2** containing EA substituents display red-shifted emission. This substituent effect is a simple and useful tool to achieve red, green, and blue emission (Fig. 1).

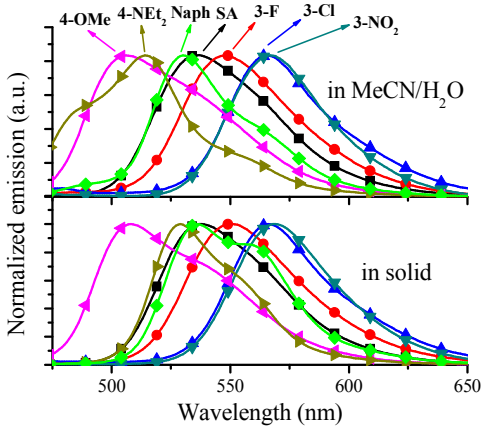

Fig. 3 Normalized emission spectra of SAs in water and solid.

It is interesting that only aggregate **3-OMe** is nonemissive. The molecule arrangements play a key role in AIE. In order to achieve high Φ, AIE-active dyes should stack closely with a short interplanar distance (d) and weak intermolecular face-to-face π–π interactions. The former can ensure to eliminate the molecular rotation, the later would prevent the formation of excimer and consequently enhance fluorescence.[8c,20] In order to investigate the molecule arrangements, the x-ray single crystals of **SA**, **4-OMe** and **3-OMe** are depicted in Fig 4, S4, and S5. All atoms in **SA** are located in one plane of π-conjugated system (Fig. 4a). As expected, the intramolecular hydrogen bonds (1.90 Å) between H atom in –OH and N atom are found in **SA**. Moreover, rod-like **SA** molecules are cross stacking with a short d of ~3.45 Å (Fig. 4c). The above two factors ensure to eliminate the rotation of N–N and C–C single bond and result in AIE thereby. However, it should be noted that there still are weak intermolecular face-to-face π–π interactions (overlaps in π-conjugated systems) between two neighbour **SA** molecules (Fig. 4b), which might be one possible reason for its moderate Φ (0.11). **4-OMe** molecules have a similar d (~3.46 Å) (Fig. 4e) but weaker face-to-face π–π interactions (Fig. 4d), and thus **4-OMe** has a higher Φ (0.16) than **SA**. On the other hand, **3-OMe** molecules have a shorter d (~3.30 Å) (Fig. 4g) but much stronger face-to-face π–π interactions (Fig. 4f), resulting in its weak fluorescence.

Another interesting phenomenon is the fact that only **4-NEt_2** displays strong fluorescence in both dilute MeCN and aggregate states. In the previous work,[20b] the strong fluorescence in solution was attributed to the intramolecular charge transfer (ICT) between D–A system[21] of the strong ED –NEt_2 substituent and EA salicylaldimine moiety, However, this can't explain the fact that **4-OMe** has strong ED substituents of –OMe as well, but it exhibits weak fluorescence

View Article Online
DOI: 10.1039/C4NJ01908C
Journal Name

in dilute MeCN. It was reported that **4-NEt$_2$** powder has two distinctive crystalline lattices with different λ_{em} at 553 (d = 3.53 Å) and 529 nm (d =6.32 Å),[20a] which are consistent with our results. The –NEt_2 substituents in **4-NEt$_2$** are much bulkier than the –OMe substituents in **4-OMe**, which might lead to reducing self quenching and consequently strong fluorescence in both solution and solid for **4-NEt$_2$**.

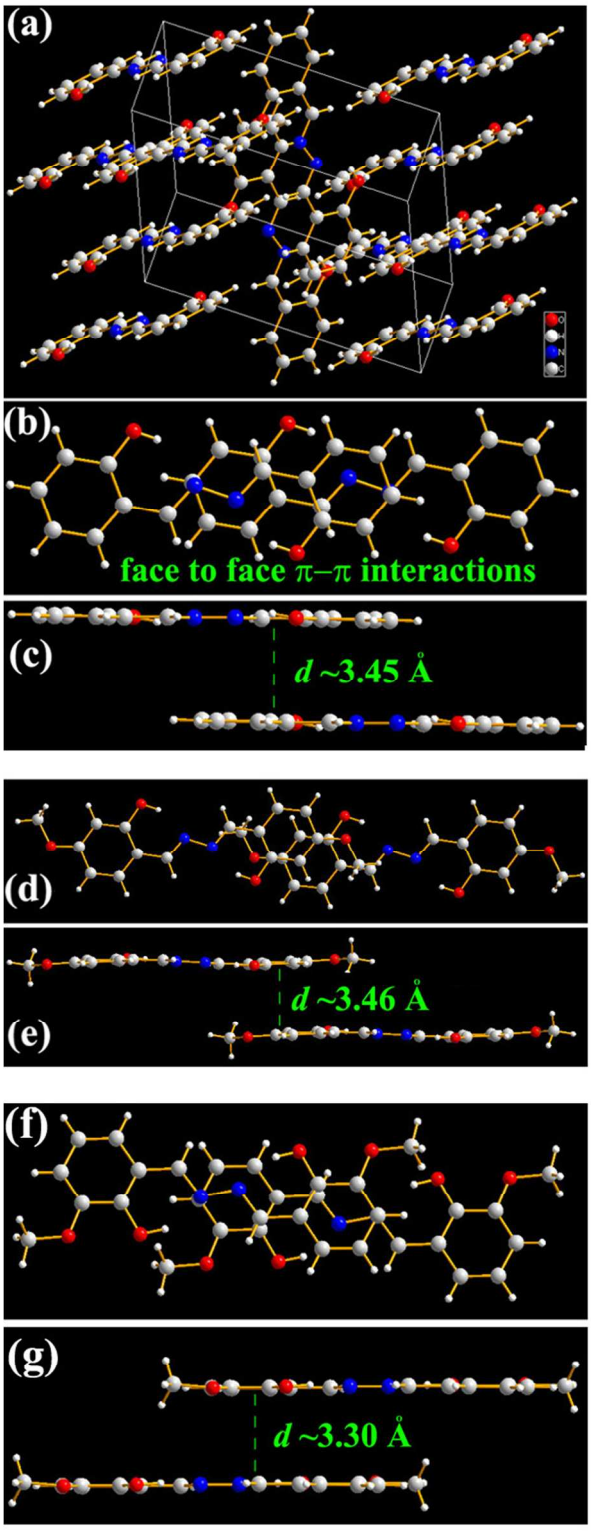

Fig. 4 X-ray single crystal structures of **SA** (a: molecule arrangement; b: top view of face-to-face π–π interactions; c: side view of face-to-face π–π interactions), **4-OMe** (d and e), and **3-OMe** (f and g).

As shown in Table 1, **Naph** has a highest Φ of 0.18 in MeCN/water. **Naph** has a similar molecule arrangement with **SA** (Fig. 5). The d (~3.10 Å) (Fig. 5c) of **Naph** molecules is the

Journal Name

View Article Online
DOI: 10.1039/C4NJ01908C

smallest. Moreover, unlike **3-OMe** molecules, **Naph** molecules almost have no face-to-face π–π interactions (Fig. 5b). Therefore, in order to enhance AIE, *d* should be short and face-to-face π–π interactions have better be weak, even though sometimes they are contradictory. The best way to solve such problem is to adopt cross molecular stacking like **Naph**. All the above discussion provides unequivocal insights into the inherent relationships between AIE properties and chemical structures and useful tools for the design of AIE-active dyes.

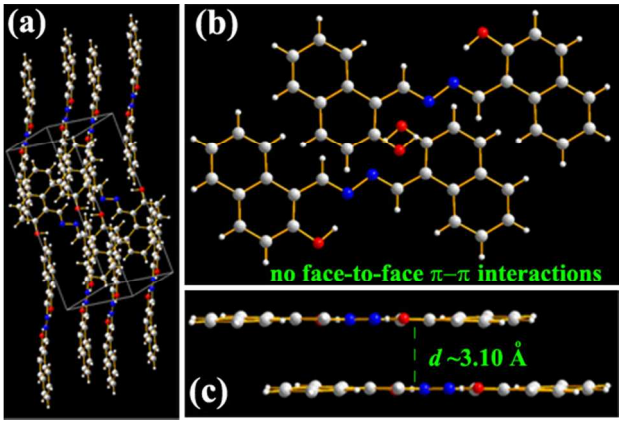

Fig. 5 X-ray single crystal structures of **Naph** (a: molecule arrangement; b: top view; c: side view).

Fluorescent pH probes

It is well-known that phenol is a weak acid with a pK_a of about 10.[22] Our previous work[9d] demonstrated that salicylaldehyde derivatives can be used as fluorescent pH probes, however, the measurement is not ratiometric fluorescence detection but turn-on or turn-off fluorescence detection.

The absorbance and fluorescence intensity of these SAs highly depend on the pH values of the solution, and thus they can be used as pH probes. The pH responses were measured in the mixed solvents of MeCN/aqueous Britton-Robinson (B-R) buffer solution (a mixture of 0.04 mol/L H_3BO_3, H_3PO_4 and CH_3COOH in water). The concentration of SAs is 1.0×10^{-5} mol dm^{-3} and the *f* is listed in Table 1. As example, the absorption (Fig. S6) and emission (Fig. 6) properties of **3-Cl** are strongly dependent on pH values. The red emission intensity at 565 nm (I_{565}) that belongs to the protonated **3-Cl** keeps constant at pH < 7.0. And then it reduces along with the increase of pH values from 7.0 to 11.0 and finally keeps constant again at pH > 11.0. At the same time, blue-green I_{515} belonging to the deprotonated **3-Cl** has a totally adverse pH response, which is zero, increased, and constant at pH < 7.0, 7.0–11.0, > 11.0, respectively (Fig. 6b). Moreover, the ration between I_{515} and I_{565} exhibits adverse pH responses with I_{565} (Fig. 6c). Therefore, **3-Cl** provides not only a ratiometric method of detection but also a perceived colour change (red to blue-green) for rapid visual sensing (Fig. 6a).

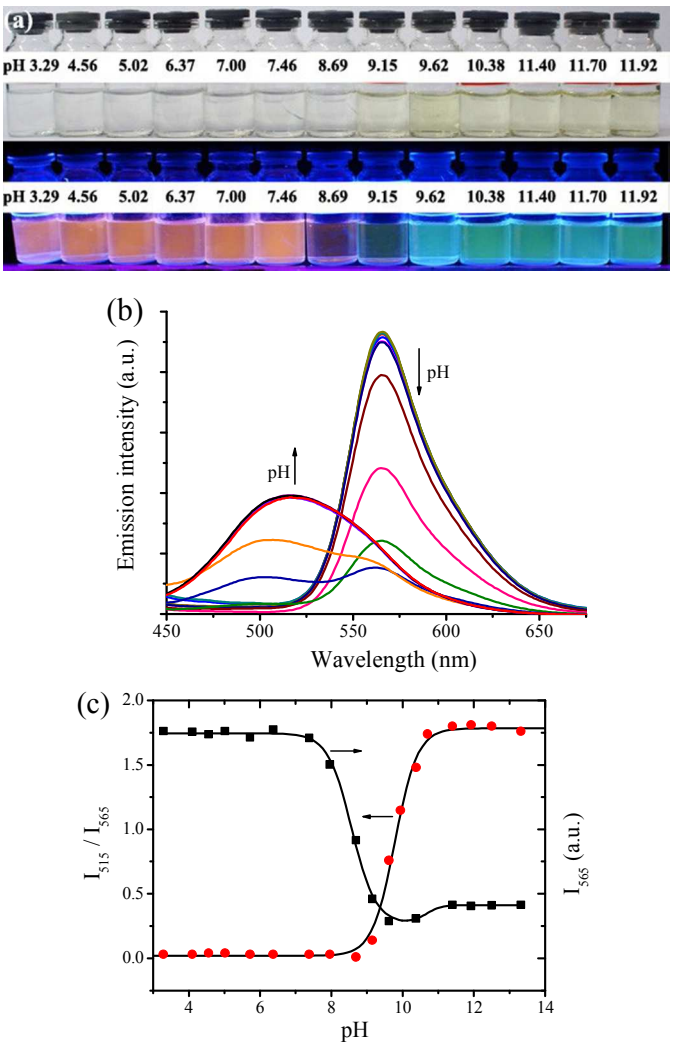

Fig. 6 Photographs (a) (top: under room light; bottom: under 360 nm UV light), emission (b) spectra, and plots (c) of I_{565} and I_{515}/I_{565} versus pH value in B-R buffer solution for **3-Cl** (1.0×10^{-5} mol dm^{-3} and $f = 94$ %).

Among these SAs, **3-Cl**, **SA**, **3-F**, and **4-OMe** exhibit ratiometric fluorescence responses to pH values (Fig. 7). Since the λ_{em} difference ($\Delta\lambda_{em}$ = 50 nm) between protonated (λ_{em} = 565 nm) and deprotonated **3-Cl** (λ_{em} = 515 nm) is bigger than that of **SA** ($\Delta\lambda_{em}$ = 23 nm, Fig. S7), **3-F** ($\Delta\lambda_{em}$ = 38 nm, Fig. S8), and **4-OMe** ($\Delta\lambda_{em}$ = 16 nm, Fig. S9), **3-Cl** is more suitable for ratiometric detection.

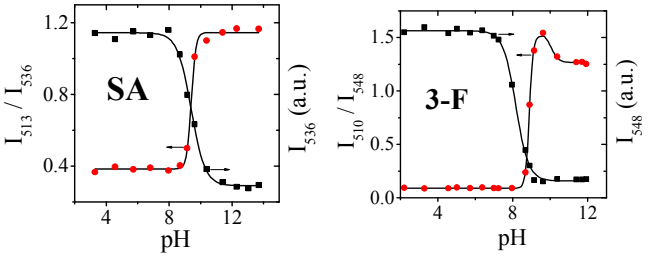

View Article Online
DOI: 10.1039/C4NJ01908C

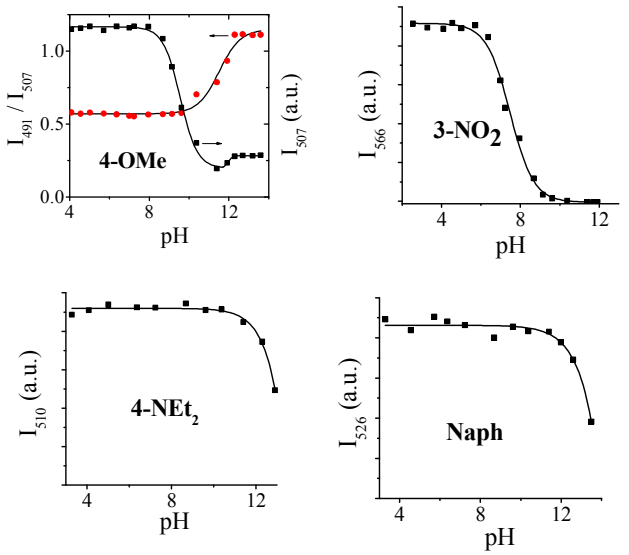

Fig. 7 Emission intensity versus pH value in B-R buffer solution for SAs (1.0×10^{-5} mol dm^{-3} and f is listed in Table 1; black and red points for intensity and ratiometric measurement, respectively).

3-OMe has too weaker fluorescence to be used as fluorescent probe. **3-NO$_2$**, **4-NEt$_2$** (Fig. 8), and **Naph** (Fig. S10) serve as turn-off fluorescent pH probes but not ratiometric fluorescent probes (Fig. 7), because they are nonemissive after deprotonation. For example, the I_{566} of **3-NO$_2$** keeps constant, decreasing, and quenching totally at pH < 5.1, 5.1–10, > 10, respectively, revealing that the pK_a of **3-NO$_2$** is 7.5 (Fig. 8). It is worthwhile that the fluorescence of **4-NEt$_2$** and **Naph** keeps constant at pH 3–10 and 3–11, respective, and then decreases upon alkalinity increase, which indicates that they can be used as fluorescent pH probes even at very high pH values. In the literature, such fluorescent probes for the detection of high pH values are still scarce. The pH values of the different subcellular compartments are 4.7–8. The pK_a values of the SAs are 7.5–13.3. And thus some of them can be potentially used in intracellular pH sensing. The pH probes with high pK_a of 9–12 might be used in some special applications, such as waste water.

It is well-known that the pK_a of phenol is about 10.[22] **SA** (pK_a = 9.3) with the presence of EA salicylaldimine moiety is more acid than phenol, because the inductive effect of EA moiety reduces the electron density of benzene ring, resulting in that the negative charge of phenolic hydroxyl will delocalize into the benzene ring. Consequently, the resultant phenolate anion is more stable and readily releases proton. On the other hand, ED substituents stress an opposite effect to decrease the acidity.

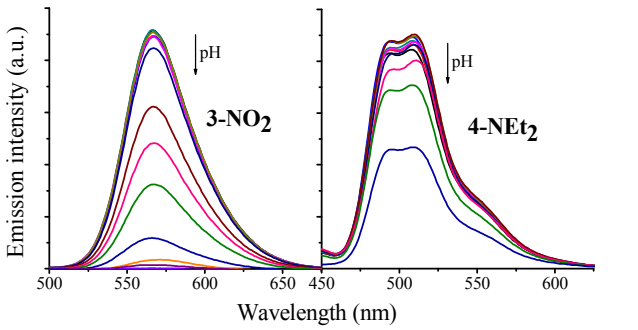

Fig. 8 Emission spectra of **3-NO$_2$** and **4-NEt$_2$** at different pH value in B-R buffer solution (1.0×10^{-5} mol dm^{-3} and f = 90 %).

Except **3-OMe**, the pK_a values (7.5–13.3) of these SAs (Table 1) were calculated by the fluorescence method. A tendency of pK_a is observed in the order of **3-NO$_2$** (pK_a = 7.5) < **3-F** (pK_a = 8.2) < **3-Cl** (pK_a = 8.5) < **SA** (pK_a = 9.3) < **4-OMe** (pK_a = 9.5) < **4-NEt$_2$** (pK_a = 13.0) < **Naph** (pK_a = 13.3), which is consistent with the fact that EA and ED substituents cause the acidity to increase and reduce, respectively, as previously mentioned. Understanding these inherent relations between chemical structures and pK_a values would be helpful to design pH probes.

Our previous work demonstrated a salicylaldehyde-based Salen Schiff base that has a similar chemical structure with SAs shows multiple different pH-sensitive segments including –OH and N=C.[9d] For **SA**, as expected, adding base would lead to the deprotonation of –OH, which can be confirmed by the ^{1}H nuclear magnetic resonance (^{1}H NMR) analysis (Fig. 9). The ^{1}H NMR signals of **SA** (δ = 11.15 ppm) in $(CD_3)_2SO$ belonging to the –OH disappear after adding base. On the contrary, there is no obvious change in the ^{1}H NMR signals if acid was added, which is consistent with the fact that the emission spectra of **SA** shows little change upon adding acid. These results reveal that, in our case, **SA** has only one type of pH-sensitive segment (–OH) to achieve ratiometric detection.

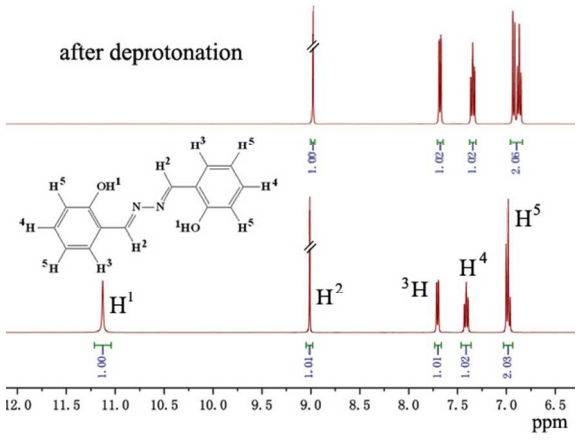

Fig. 9 ^{1}H NMR spectra of **SA** (bottom) and deprotonated **SA** (top, adding 2 equiv. of NaOH in D_2O) in $(CD_3)_2SO$.

Journal Name

View Article Online
DOI: 10.1039/C4NJ01908C

The previous work[10a] observed that **SA** molecules aggregate in water to form nanoparticles (<5 nm), which reveals **SA** molecules are not dissolved but disperse in water. One of problems of these nanoparticles without any surface protective agents is that the disperse nanoparticles are not stable and would precipitate through further aggregation. Therefore, the dynamic stability of **3-Cl** nanoparticles in MeCN/water was examined (Fig. 10). After adding water to the MeCN solution of **3-Cl**, the emission of **3-Cl** reaches saturation (> 95 %) in 15 minutes, indicating that **3-Cl** molecules aggregate to form nanoparticles very quick. Moreover, the nanoparticles are stable at least 150 minutes, which is enough for sensing applications.

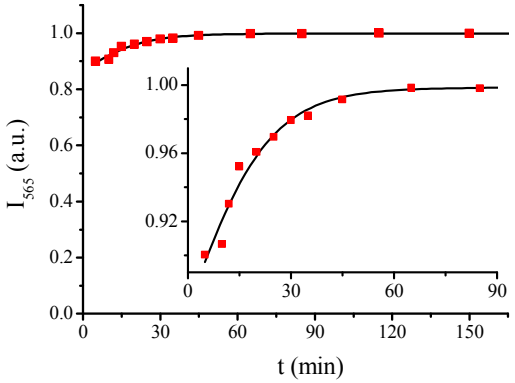

Fig. 10 Kinetics of I_{565} for **3-Cl** in MeCN/water (1.0×10^{-5} mol dm^{-3}, f = 94 %).

pH test paper

One of the best superiorities of AIE-active dyes is the nature of strong fluorescence in solid, and thus we tried to use **3-Cl** as pH test papers. The homemade test papers were fabricated by dipping filter papers into the MeCN solution of **3-Cl**. When the solvent evaporates, the adsorbed **3-Cl** molecules in the test paper aggregate to emit strong red fluorescence like that in MeCN/water solutions (Fig. 11). This aggregation is also confirmed by the fact that the red fluorescence don't distribute uniformly in the test paper under UV irradiation. When the test papers are dipped into aqueous B-R buffer solution with different pH values, they exhibit different color changes under room light and 360 nm UV light, respectively. Under room light, the color of test papers changes from white into yellow at high pH values, which accords with the absorption enhancement at high pH values (Fig. S6). Under UV irradiation, the test papers appear a much more obvious color change. The test papers display red, yellow, and green fluorescence at pH values of 6–9, 10–11, and 12–14, respectively. It should be noted that the test papers emit green fluorescence at high pH values, at the same condition, however, the MeCN/water solutions display blue-green fluorescence (Fig. 6a). At high pH values, **3-Cl** would be deprotonated to form phenolate consequently, which has a better solubility and less AIE effect than protonated **3-Cl** in water. This less AIE effect is coincident with the fact that the green fluorescence from test papers containing deprotonated **3-Cl** is more uniform (Fig. 11). Since deprotonated **3-Cl** is a traditional organic dye rather than an AIE-active dye, its fluorescence in solid is red-shifted compared with that in the dilute solution.

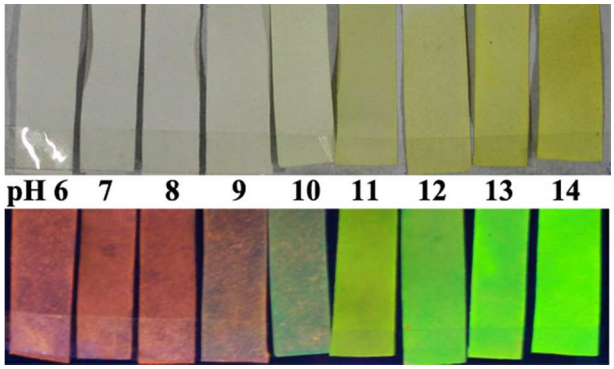

Fig. 11 Colour changes (top: under room light; bottom: under 360 nm UV light) of homemade **3-Cl** test papers at different pH values.

Conclusion

We have systematically synthesized and studied the photophysical properties and pH sensing applications of a series of salicylaldehyde azines. The chemical structures of these salicylaldehyde azines have a significant influence on their molecule arrangements and consequently aggregation-induced emission properties. Strong cross stacking of molecule arrangement with a small d and weak face-to-face π–π interactions is a key factor to enhance aggregation-induced emission. **3-Cl**, **3-F**, and **4-OMe** exhibit aggregation-induced emission at low pH values, while they become water soluble and show blue-shifted fluorescence at high pH values, and thus they can be used as ratiometric fluorescent pH probes with a broad pH range in water and solid (test paper). Moreover, their pK_a values ranging from 7.5 to 13.3 can be varied and well tuned by their chemical structures. Therefore, we believe that these simple salicylaldehyde azines provide a new paradigm in the design of aggregation-induced emission-active dyes for some useful sensing applications.

Experimental section

Materials and instrumentation

All reagents were purchased from commercial suppliers and used without further purification. UV/visible absorption spectra were recorded using a UV 765 spectrophotometer with quartz cuvettes of 1 cm pathlength. Fluorescence spectra were obtained using an F-7000 Fluorescence spectrophotometer (Hitachi) at room temperature. The slit width was 2.5 or 5.0 nm for both excitation and emission. The photon multiplier voltage was 400 V. All SAs were prepared according to the previous reports.[19] The X-ray structures of SA,[23a] 3-OMe,[23b] 4-OMe,[23c] and Naph[23d] were previously reported.

Measurement of fluorescence quantum yield (Φ)

View Article Online
DOI: 10.1039/C4NJ01908C
Journal Name

Φ was measured by the optical dilute method with a standard of quinine sulfate (Φ_r = 0.55, quinine in 0.05 mol dm^{-3} sulfuric acid) calculated by: $\Phi_s = \Phi_r (B_r/B_s) (n_s/n_r)^2 (D_s/D_r)$, where the subscripts s and r refer to the sample and reference standard solution respectively; *n* is the refractive index of the solvents; D is the integrated intensity. The excitation intensity *B* is calculated by: $B = 1 - 10^{-A\,L}$, where A is the absorbance at the excitation wavelength and L is the optical path length (L = 1 cm in all cases). The refractive indices of the solvents at room temperature are taken from standard source. Errors for Φ values (± 10%) are estimated.

Measurement of pH sensing

The pH responses were measured in the mixed solvents of MeCN/aqueous B-R buffer solution (a mixture of 0.04 mol/L H_3BO_3, H_3PO_4 and CH_3COOH in water). The concentration of SAs is 1.0×10^{-5} mol dm^{-3} and the *f* is listed in Table 1. All types of absorption and fluorescence measurement were monitored 1 hour after the addition of the probe to the buffer solution at room temperature.

Synthesis

N,N'-bis(salicylidene) hydrazine (SA).[19] 30 ml ethanol of aqueous hydrazine (5 mmol, 0.25 g) was added into 20 ml ethanol of salicylaldehyde (10 mmol, 1.22 g) over a period of 1 h, and then the mixture was refluxed for 4 h. The solution was concentrated to give crude solid, which was recrystallized from ethanol and dried to get 0.92 g (77 % yield) of compound as a pale yellow solid; ^{1}H NMR (DMSO-d_6, 400 MHz): δ (ppm) 11.13 (s, 2H), 9.01 (s, 2H), 7.69–7.72 (m, 2H), 7.38–7.43 (m, 2H), 6.95–7.01 (m, 4H). Anal. Calcd (found): C, 69.99 (69.74); H, 5.03 (4.86); N, 11.66 (11.64). ESI-MS, m/z 240.3.

N,N'-bis(3-fluoro salicylidene) hydrazine (3-F).[19] **3-F** was prepared by a similar procedure as that used for SA, but with 3-fluoro-salicylaldehyde (10 mmol, 1.40 g) to give pale yellow solid 1.01 g (73 % yield); m.p. 265 °C. ^{1}H NMR (DMSO-d_6, 400 MHz): δ (ppm) 11.31 (s, 2H), 9.09 (s, 2H), 7.54–7.56 (d, 2H), 7.38–7.43 (m, 2H), 6.96–7.01 (m, 2H). ^{13}C NMR (DMSO-d_6, 400 MHz): δ (ppm) 119.76 120.02 121.13 126.68 146.95 151.38 163.37. Anal. Calcd (found): C, 60.87 (60.74); H, 3.65 (3.69); N, 10.14 (10.04). ESI-MS, m/z 276.1.

N,N'-bis(3-chloro salicylidene) hydrazine (3-Cl).[19] **3-Cl** was prepared by a similar procedure as that used for SA, but with 3-chloro-salicylaldehyde (10 mmol, 1.56 g) to give pale yellow solid 1.22 g (79 % yield); ^{1}H NMR (DMSO-d_6, 400 MHz): δ (ppm) 11.90 (s, 2H), 9.14 (s, 2H), 7.61–7.65 (m, 4H), 7.03–7.07 (m, 2H). Anal. Calcd (found): C, 54.39 (54.28); H, 3.26 (3.14); N, 9.06 (9.04). ESI-MS, m/z 308.

N,N'-bis(3-nitro salicylidene) hydrazine (3-NO_2).[19] **3-NO_2** was prepared by a similar procedure as that used for SA, but with 3-nitro-salicylaldehyde (10 mmol, 1.67 g) to give yellow solid 1.15 g (70 % yield); Anal. Calcd (found): C, 50.92 (50.80); H, 3.05 (3.00); N, 16.96 (16.86).

N,N'-bis(3-methoxyl salicylidene) hydrazine (3-OMe).[19] **3-OMe** was prepared by a similar procedure as that used for SA, but with 3-methoxyl -salicylaldehyde (10 mmol, 1.13 g) to give pale yellow solid 1.08 g (75 % yield); ^{1}H NMR (DMSO-d_6, 400 MHz): δ (ppm) 10.90 (s, 2H), 9.00 (s, 2H), 7.28–7.31 (m, 2H), 7.12–7.15 (m, 2H), 6.90–6.94 (m, 2H), 3.84 (s, 6H). Anal. Calcd (found): C, 63.99 (63.78); H, 5.37 (5.14); N, 9.33 (9.14). ESI-MS, m/z 300.

N,N'-bis(4-methoxyl salicylidene) hydrazine (4-OMe).[19] **4-OMe** was prepared by a similar procedure as that used for SA, but with 4-methoxyl -salicylaldehyde (10 mmol, 1.11 g) to give pale yellow solid 1.08 g (74 % yield); ^{1}H NMR (DMSO-d_6, 400 MHz): δ (ppm) 11.52 (s, 2H), 8.87 (s, 2H), 7.54–7.56 (d, 2H), 6.57–6.59 (m, 2H) , 6.52–6.54 (d, 2H), 3.81 (s, 6H). Anal. Calcd (found): C, 63.99 (63.91); H, 5.37 (5.23); N, 9.33 (9.25). ESI-MS, m/z 300.

N,N'-bis(4-diethylamino salicylidene) hydrazine (4-NEt_2).[19] **4-NEt_2** was prepared by a similar procedure as that used for SA, but with 4-diethylamino-salicylaldehyde (10 mmol, 1.93 g) to give yellow solid 1.38 g (72 % yield); ^{1}H NMR (DMSO-d_6, 400 MHz): δ (ppm) 11.50 (s, 2H), 8.62 (s, 2H), 7.26–7.31 (d, 2H), 6.29–6.53 (d, 2H), 6.12 (s, 2H), 3.19–3.25 (q, 8H), 1.09–1.14 (t, 12H). Anal. Calcd (found): C, 69.08 (69.17); H, 7.91 (7.87); N, 14.65 (14.60). ESI-MS, m/z 382.2.

2,2'-dihydroxy-1,1'-naphthalazine (Naph).[19] **Naph** was prepared by a similar procedure as that used for SA, but with 2-hydroxy-1-naphthaldehyde (10 mmol, 1.72 g) to give yellow solid 1.02 g (60 % yield); ^{1}H NMR (DMSO-d_6, 400 MHz): δ (ppm) 12.88 (s,2H) , 10.00 (s, 2H) , 8.65 (d, 2H) , 8.01 (m, 2H) , 7.92 (m, 2H) , 7.63 (m, 2H) , 7.45 (m, 2H) , 7.28 (m, 2H). Anal. Calcd (found): C, 77.63 (77.91); H, 4.74 (4.77); N, 8.23 (8.28). ESI-MS, m/z 340.1.

Acknowledgements

This work was supported by the National Natural Science Foundation of China (no. 21172160 and 21372169).

Notes and references

College of Chemistry, Sichuan University, Chengdu, 610041, China. Fax: (+86) 28-8541-2291. E-mail: xianghaifeng@scu.edu.cn.

Electronic Supplementary Information (ESI) available: Photophysical properties and applications of fluorescent pH probes of SAs. See DOI: 10.1039/b000000x/

1 A. S. Vasylevska, A. A. Karasyov, S. M. Borisov and C. Krause, *Anal. Bioanal. Chem.,* 2007, **387**, 2131.

2 (a) J. Srivastava, D. L. Barber and M. P. Jacobson, *Physiology*, 2007, **22**, 30; (b) R. Wang, C. W. Yu, F. B. Yu and L. X. Chen, *TrAC, Trends Anal. Chem.*, 2010, **29**, 1004. (c) J. Y. Han, K. Burgess, *Chem. Rev.,* 2010, **110**, 2709.

3 Y. Feng, J. H. Cheng, L. Zhou, X. G. Zhou and H. F. Xiang, *Analyst,* 2012, **137**, 4885.

4 (a) C. G. Niu, X. Q. Gui, G. M. Zeng and X. Z. Yuan, *Analyst*, 2005, **130**, 1551; (b) H. S. Peng, J. A. Stolwijk, L. N. Sun, J. Wegener and

Journal Name View Article Online DOI: 10.1039/C4NJ01908C ARTICLE

O. S. Wolfbeis, *Angew. Chem. Int. Ed.*, 2010, **49**, 4246; (c) S. Wu, Z. Li, J. Han and S. Han, *Chem. Commun.*, 2011, **47**, 11276; (d) D. Aigner, B. Ungerbock, T. Mayr, R. Saf, I. Klimant and S. M. Borisov, *J. Mater. Chem. C*, 2013, **1**, 5685.

5 (a) S. Chen, Y. Hong, Y. Liu, J. Liu, C. W. T. Leung, M. Li, R T. K. Kwok, E. Zhao, J. W. Y. Lam, Y. Yu and B. Z. Tang, *Chem. Sci.*, 2012, **3**, 1804; (b) M. H. Lee, J. H. Han, J. H. Lee, N. Park, R. Kumar, C. Kang and J. S. Kim, *Angew. Chem. Int. Ed.*, 2013, **52**, 6206; (c) G. Men, G. Zhang, C. Liang, H. Liu, B. Yang, Y. Pan, Z. Wang and S. Jiang, *Analyst*, 2013, **138**, 2847; (d) X. D. Liu, Y. Xu, R. Sun, Y. J. Xu, J. M. Lu and J. F. Ge, *Analyst*, 2013, **138**, 6542; (e) S. Chen, Y. Hong, Y. Liu, J. Liu, C. W. T. Leung, M. Li, R. T. K. Kwok, E. Zhao, J. W. Y. Lam, Y. Yu and B. Z. Tang, *J. Am. Chem. Soc.*, 2013, **135**, 4926; (f) P. Y. Gu, J. Gao, Q. Zhang, G. Liu, F. Zhou, Q. F. Xu and J. M. Lu, *J. Mater. Chem. C*, 2014, **2**, 1539.

6 (a) C. K. Koo, B. Lam, S. K. Leung, M. H. W. Lam and W. Y. Wong, *J. Am. Chem. Soc.*, 2006, **128**, 16434; (b) R. Pal and D. Parker, *Chem. Commun.*, 2007, 474; (c) J. Wang, Y. Sun, W. Zhang, Y. Liu, X. Yu and N. Zhao, *Talanta*, 2014, 129, 241.

7 J. Luo, Z. Xie, J. W. Y. Lam, L. Cheng, B. Z. Tang, H. Chen, C. Qiu, H. S. Kwok, X. Zhan, Y. Liu and D. Zhu, *Chem. Commun.*, 2001, 1740.

8 (a) Y. Hong, J. W. Y. Lam and B. Z. Tang, *Chem. Commun.*, 2009, 4332; (b) M. Wang, G. Zhang, D. Zhang, D. Zhu and B. Z. Tang, *J. Mater. Chem.*, 2010, **20**, 1858; (c) Y. Hong, J. W. Y. Lam and B. Z. Tang, *Chem. Soc. Rev.*, 2011, **40**, 5361.

9 (a) L. Zhou, P. Y. Cai, Y. Feng, J. H. Cheng, H. F. Xiang, J. Liu, D. Wu and X. G. Zhou, *Anal. Chim. Acta*, 2012, **735**, 96; (b) L. Zhou, Y. Feng, J. H. Cheng, N. Sun, X. G. Zhou and H. F. Xiang, *RSC Adv.*, 2012, **2**, 10529; (c) J. H. Cheng, K. Y. Wei, X. F. Ma, X. G. Zhou and H. F. Xiang, *J. Phys. Chem. C*, 2013, **117**, 16552; (d) J. H. Cheng, Y. H. Zhang, X. F. Ma, X. G. Zhou and H. F. Xiang, *Chem. Commun.*, 2013, **49**, 11791; (e) J. H. Cheng, X. F. Ma, Y. H. Zhang, J. Y. Liu, X. G. Zhou and H. F. Xiang, *Inorg. Chem.*, 2014, **53**, 3210.

10 (a) W. Tang, Y. Xiang and A. Tong, *J. Org. Chem.*, 2009, **74**, 2163; (b) R. Wei, P. Song and A. Tong, *J. Phys. Chem. C*, 2013, **117**, 3467; (c) X. Chen, A. Tong, *J. Lumin.*, 2014, **145**, 737; (d) L. Peng, Z. Zhou, R. Wei, K. Li, P. Song and A. Tong, *Dyes Pigments*, 2014, **108**, 24.

11 M. Ziolek, M. Gil, J. A. Organer and A. Douhal, *Phys. Chem. Chem. Phys.*, 2010, **12**, 2107.

12 (a) D. X. Xie, Z. J. Ran, Z. Jin, X. B. Zhang and D. L. An, *Dyes Pigments*, 2013, **96**, 495; (b) X. Cao, X. Zeng, L. Mu, Y. Chen, R. Wang, Y. Zhang, J. Zhang and G. Wei, *Sens. Actuators B: Chem.*, 2013, **177**, 493.

13 S. Dalapati, S. Jana, Md. A Alam and Ni. Guchhait, *Sens. Actuators B: Chem.*, 2011, **160**, 1106.

14 Q. Li, Y. Guo, Ji. Xu and S. Shao, *Sens. Actuators B: Chem.*, 2011, **158**, 427.

15 (a) W. T. Gong, Q. L. Zhang, L. Shang, B. Gao and G. L. Ning, *Sens. Actuators B: Chem.*, 2013, **177**, 322; (b) P. Zhang, B. B. Sh, X. M. You, Y. M. Zhang, Q. Lin, H. Yao and T. B. Wei, *Tetrahedron*, 2014, **70**, 1889.

16 L. Peng, R. Wei, K. Li, Z. Zhou, P. Song and A. Tong, *Analyst*, 2013, **138**, 2068.

17 H. Liu,P. Song, R. Wei, K. Li and A. Tong, *Talanta*, 2014, **118**, 348.

18 (a) Z. Li, Y. Q. Dong, J. W. Y. Lam, J. Sun, A. Qin, M. Hauler, Y. P. Dong, H. H. Y. Sung, I. D. Williams, H. S. Kwok and B. Z. Tang, *Adv. Funct. Mater.*, 2009, **19**, 905; (b) Z. Yang, W. Qin, J. W. Y. Lam, S. Chen, H. H. Y. Sung, I. D. Williams and B. Z. Tang, *Chem. Sci.*, 2013, **4**, 3725.

19 H. Gorner, S. Khanra, T. Weyhermuller and P. Chaudhuri, *J. Phys. Chem. A*, 2006, **110**, 2587.

20 (a) X. Chen, R. Wei, Y. Xiang, Z. Zhou, K. Li, P. Song and A. Tong, J. *Phys. Chem. C*, 2011, **115**, 14353; (b) S. Jana, S. Dalapati, and N. Guchhait, *J. Phys. Chem. A*, 2012, **116**, 10948.

21 H. F. Xiang, J. H. Cheng, X. F. Ma, X. G. Zhou and J. J. Chruma, *Chem. Soc. Rev.*, 2013, **42**, 6128

22 K. Gross and P. G. Seybold, *Int. J. Quantum. Chem.*, 2001, **85**, 569.

23 (a) X. X. Xu, X. Z. You, Z. F. Sun, X. Wang and H. X. Liu, *Acta Cryst. C*, 1994, **50**, 1169; (b) S. G. Teoh, S. B. Teo, G. Y. Yeap and H. K. Fun, *Main Group Met. Chem.*, 1994, **17**, 595; (c) H. Takakashi, K. Kubo, H. Takechi, T. Matsumoto and K. Ideta, *Yukagaku*, 2006, **55**, 483; (d) D. Guo, J. H. Li, J. J. Xie, C. Y. Duan, Q. J. Meng, *Chin. J. Inorg. Chem.*, 2002, **18**, 1215.